739

Cyclic compressive behavior of polyurethane rubber springs for smart dampers

Eunsoo Choi[1a], Jong-Su Jeon [2b] and Junwon Seo[*3]

[1]*Department of Civil Engineering, Hongik University, Seoul 04066, Korea*
[2]*Department of Civil Engineering, Andong National University, Andong, Gyeongsanbuk-do 36729, Korea*
[3]*Department of Civil and Environmental Engineering, South Dakota State University, Brookings, SD 57007, USA*

Abstract. The main goal of this study is to investigate the hysteretic behavior of polyurethane rubber springs in compression with and without precompression. The precompression is introduced to provide rigid force in the behavior, and thereby a precompressed rubber spring can be used for a restoring element. For the goal, this study prepares nine rubber springs for three suites which are all cylindrical in shape with a hole at the center. The rubber springs in each suite have different dimensions of diameter and length but have similar shape factors; thus, they are designed to have a similar compressive stiffness. Three rubber springs from the nine are tested with increasing compressive strain up to 30% strain to investigate the behavior of the rubber springs without precompression as well as the effect of the loading strain. The nine springs are compressed up to 30% strain with increasing precompressive strain from 0 to 20% at increments of 5%. The study analyzes the effective stiffness and damping ratio of the rubber springs with and without precompression, and the rigid force of the precompressed rubber springs is discussed. Finally, this study suggests a regression method to determine the minimum required precompression to eliminate residual strain after unloading.

Keywords: rubber spring; hysteretic behavior; precompression; self-centering; smart damper

1. Introduction

Rubber is commonly used for vibration isolation and energy dissipation in mechanical and structural systems. In civil engineering, natural rubber is employed for supporting structures (Strauss *et al*. 2014, Kim *et al*. 2004) and seismic isolation devices in the form of bearings (Bhuiyan and Alam 2013, Hwang *et al*. 2002, Kikuchi and Aiken 1997). However, natural rubber reveals low hardness, ranging from 50A to 70A on a durometer scale, and results in relatively low stiffness in compression (Oh *et al*. 2005). Thus, natural rubber pads should be reinforced by steel shims or fiber-reinforced-polymer (FRP) plates when used for structural bearings (Pauletta *et al*. 2015, Dezfuli and Alam 2013). In recent times, to overcome this problem, polyurethane rubber has been applied to structural bearings without any reinforcement inside (Oh *et al*. 2006, Choi *et al*. 2006).

Polyurethane rubber shows a relatively high hardness of 60A to 70D on a durometer scale. Thus, polyurethane rubber among other elastomers shows high compressive stiffness accompanied by high anti-abrasion performance, and results in a wide range of applications from commercial products to parts for mechanical devices (Qi and Boyce 2005).

One of the most popular applications of polyurethane rubber is in springs. Most polyurethane springs utilize a cylindrical shape. One application of polyurethane rubber springs in civil engineering is in the Eradi-Quake System (EQS), a kind of seismic isolation device generally used for bridges and buildings. Recently, the EQS device was used to isolate a nuclear island that included a nuclear reactor, cooling tower, and generator. The polyurethane rubber springs in the EQS device provide a self-centering force after sliding due to an earthquake. However, the polyurethane rubber springs in the EQS do not recover whole sliding displacement, and there remains residual displacement after an earthquake. It was understood that polyurethane rubber springs with precompression resulted in a flag-shaped behavior and provided a perfect self-centering capacity; this is one of the critical factors of smart dampers or devices for seismic isolation. They compared the behaviors of polyurethane rubber springs with and without precompression. The precompression of the rubber springs removed residual deformation and provided rigid force with a flag-shape. Thus, the behavior of precompressed polyurethane rubber springs is similar to that of superelastic shape memory alloy (SMA) wires, which are considered a smart material (Kan *et al.* 2016, Reedlunn *et al.* 2013, Attanasi and Auricchio 2011). Before Choi's study, several studies used superelastic NiTi SMA wires to provide self-centering capacity for a smart damper (Dole *et al.* 2000, Ozbulut and Herlebaus 2011, Soul and Yawny 2015, Qiu and Zhu 2017). Alipour *et al.* (2017) used

---

∗Corresponding author, Assistant Professor
  E-mail: junwon.seo@sdstate.edu
[a] Professor
  E-mail: eunsoochoi@hongik.ac.kr
[b] Assistant Professor
  E-mail jsjeon@anu.ac.kr

pre-stretched superelastic SMA wire for a self-centering damper, in which the first part of elastic range of the superelastic SMA wire was disappeared due to the pre-stretching; this increased the self-centering capacity and damping ration of the damper. In recent, superelastic SMA rings have been used for self-centering of devices or structures (Fang *et al.* 2015, Gao *et al.* 2016); it is found that the SMA rings were effective to provide self-centering capacity in multi-direction because of their bi-symmetric shape. However, the price of polyurethane rubber is much cheaper than that of NiTi SMAs. Additionally, rubber springs are activated only in compression, while SMA wires are activated only in tension. A tensioning device is mechanically difficult to realize because of the holding of the wires (Dole *et al.* 2005, Dhar *et al.* 2015). A compression device is easily embodied by contacting two surfaces. Thus, polyurethane rubber springs with precompression are considered to be more practical for smart dampers or other devices.

The aim of this study is to investigate the compressive behavior of polyurethane rubber springs with and without precompression. For this, three different compressive stiffnesses of rubber springs were considered, and three cylindrical rubber springs were prepared for each case of stiffness by varying length and cross-sectional area of the rubber springs. This study analyzed rigid force, energy dissipation, and stiffness variation due to the amount of precompression.

2. Polyurethane rubber springs

This study prepared cylindrical polyurethane rubber springs with a hole at the center, as shown in Fig. 1. First, the rubber cylinder was made with a long length using pultrusion, and, then, it was cut by a specific length to make rubber springs. Finally, the top and bottom of the spring were treated with ruggedness to provide more frictional resistance. The durometer hardness of the polyurethane rubber was 95A, which is much greater than that of natural rubber (Oh *et al.* 2005); their durometer hardness ranges from 50A to 70A. As a result, polyurethane rubber can be applied to stiffer springs than natural rubber because higher hardness rubber generally shows a higher elastic modulus.

The diameter of the hole inside was fixed at 20 mm for all of the springs since a shaft for compression should be inserted into the hole. This study considered three lengths of rubber springs, namely 80, 90, and 100 mm, respectively, and three suites of springs with different compressive stiffness were prepared. Each suite contained three springs with different lengths, and they were designed to have an identical compressive stiffness by controlling the shape factor of the rubber springs; thus, the rubber springs in one suite had similar shape factors. There were a total of nine specimens of rubber springs, and a suite of three specimens with different lengths had an identical compressive stiffness (see Fig. 1). The compressive stiffness k of the rubber springs can be assessed as

$$k = \frac{E_a A}{L} \qquad (1)$$

where E_a is the apparent elastic modulus of the rubber, and L and A are the length and cross-sectional area of the rubber spring, respectively. To obtain equal stiffness for the springs in a suite, the cross-sectional area A in Eq. (1) should be controlled by considering the length L. Thus, the outside diameter D_1 was controlled, since the inside diameter D_2 was fixed. Table 1 illustrates the outside diameters of the rubber springs with their shape factors S, which is calculated as

$$S = \frac{loaded \cdot area}{force \cdot free \cdot area} \qquad (2)$$

The outside diameter D_1 was determined on the assumption that the E_a in Eq. (1) is identical for springs in a suite. However, it is well-known that the apparent elastic modulus of rubber springs is a function of the shape factor. There is a small difference in compressive stiffness of springs in a suite since the shape factors deviated, ranging from 2.2% to 9.5%. The elastic modulus of polyurethane rubber E_o was estimated from the author's previous study as 52.8 MPa. Then, the apparent elastic modulus can be estimated using the following equation (Koblar *et al.* 2014):

$$E_a = E_o(1.2 + 2S^2) \qquad (3)$$

Table 1 also shows the estimated apparent elastic modulus and compressive stiffness of the springs, and the deviation of the stiffness between the springs in a suite is lower than 2.5%; the shorter length spring in a suite showed greater stiffness. In Table 1, the average compressive stiffnesses of the springs in Suite-II and -III are 2.38 and 3.12 times of that of the springs in Suite-I, respectively.
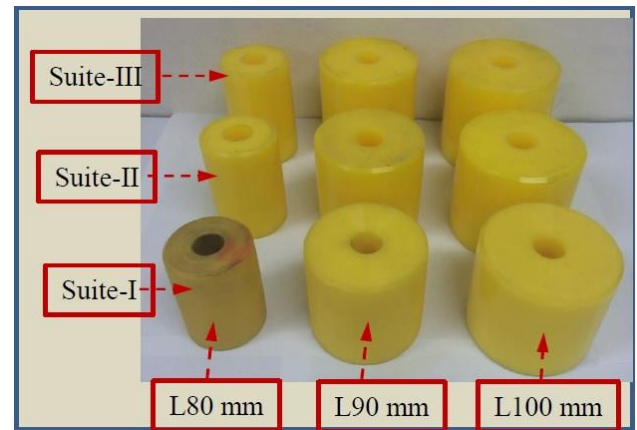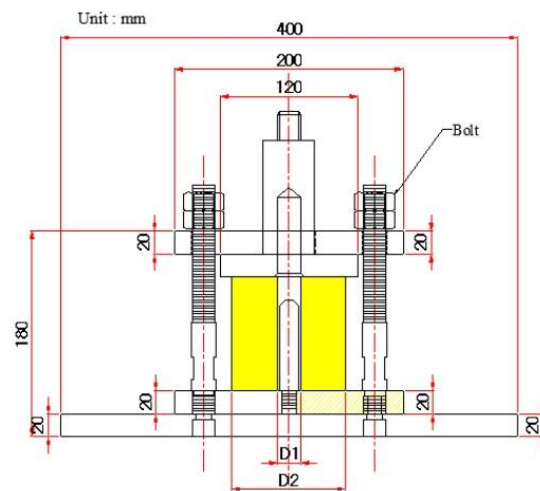

Fig. 1 Polyurethane rubber springs in the three suits

Table 1 Dimensions and calculated compressive stiffness of polyurethane rubber springs

Suite	Specimen	Length (mm)	Outer diameter (mm)	Inner diameter (mm)	Shape factor	E_a (MPa)	k_c (kN/mm)
Suite- I	80L-55D	80	55		0.109	64.62	1.665
	90L-58D	90	58	20	0.104	64.50	1.629
	100L-60D	100	60		0.102	64.45	1.661
Suite- II	80L-80D	80	80		0.188	67.07	3.951
	90L-85D	90	85	20	0.179	66.76	3.933
	100L-89D	100	89		0.172	66.49	3.917
Suite- III	80L-90D	80	90		0.219	68.41	5.172
	90L-95D	90	95	20	0.209	67.97	5.138
	100L-100D	100	100		0.200	67.60	5.109

(a) Drawing with dimension

(b) Initial state

(c) Compressed state

Fig. 2 Test set-up for compression of rubber springs

3. Test set-up and experimental program

To conduct the compressive tests of the rubber springs, a special device with two sole plates and four shafts was manufactured, and the shafts were mounted on the bottom plate (see Fig. 2). A rubber spring was placed between the two sole plates (see Fig. 2(b)), and the top plate moved by sliding on the shafts during compression (see Fig. 2(c)). The sole plates had a projecting part inserted into the inner hole

at the top and bottom of the rubber spring and resisted lateral movement of the spring. To introduce precompression, the rubber spring was first pressed by the actuator and then held by bolts on the shafts. A displacement transducer was installed between the two sole plates to measure the deformation of the rubber spring, and a load cell in the actuator measured the loading force.

The tests were conducted with varying precompressive strain from 0 to 20% with increments of 5%; the strain was
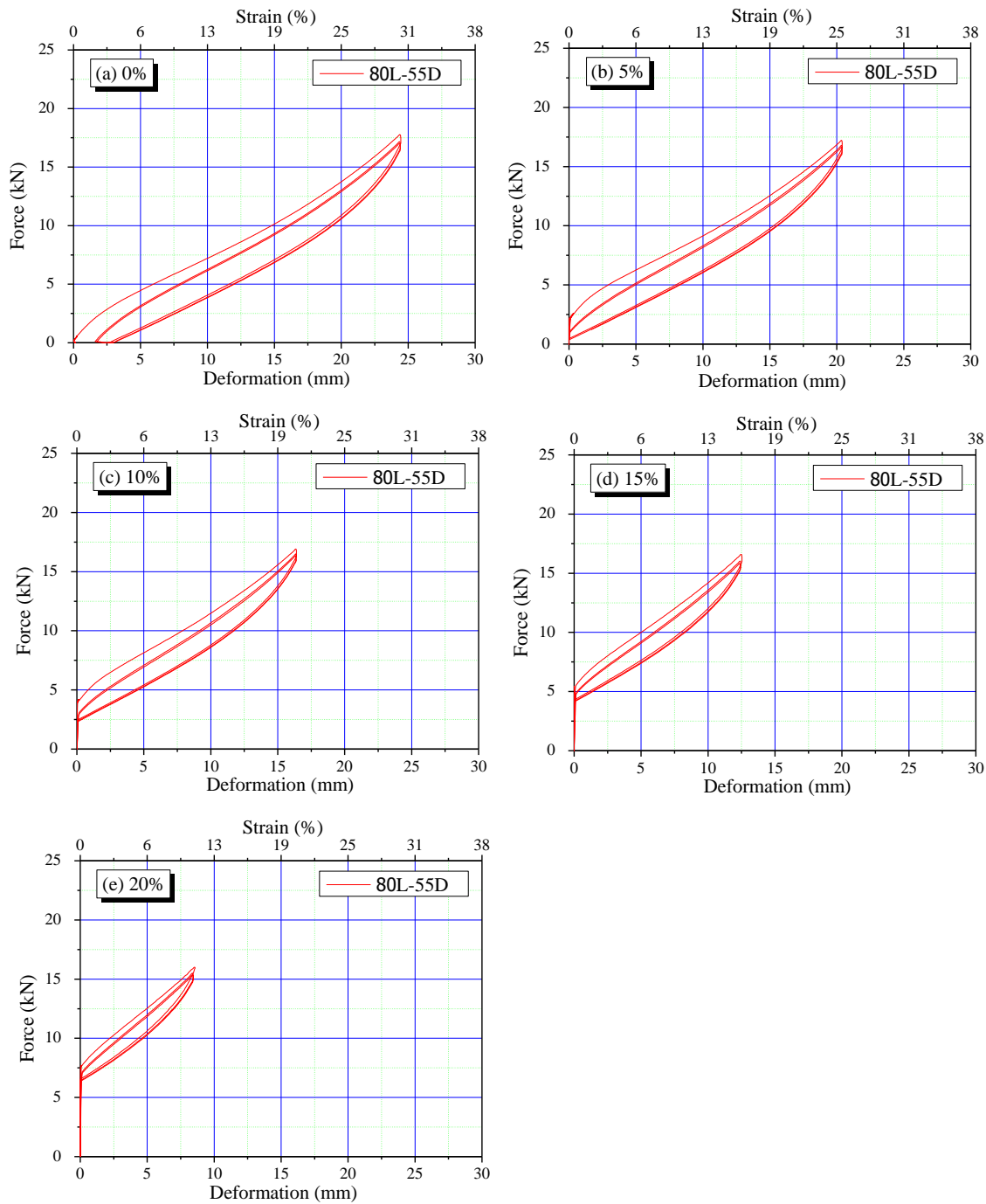
Fig. 3 Hysteretic curves of the 80L-55D specimen in Suite-I

calculated by dividing precompressive deformation by the initial length of a rubber spring. The total compressive deformation was fixed to 30% strain, and thus, when precompression is applied, the additional compressive deformation is reduced from 30% strain by the precompressive strain; for example, when the precompressive strain is 5%, the additional compressive strain will be 25% (30%-5%). It is judged from the experiment that the 30% compressive strain was considered as the maximum strain for the application of the springs. It was observed that when the total compressive strain

exceeds 30% strain, a serious degradation of strength occurred. Three cyclic loadings were applied in the test. The speed of the stroke was fixed at 4 mm/sec for all springs; thus, the loading frequency varied with the length of the spring and the total compressive strain. For example, for the 80 mm spring without precompression, the loading frequency was 0.083 Hz while the frequency was 0.25 Hz for the same spring with 20% precompressive strain; this was the highest loading frequency. Thus, the loading frequencies for all of the springs were slow.
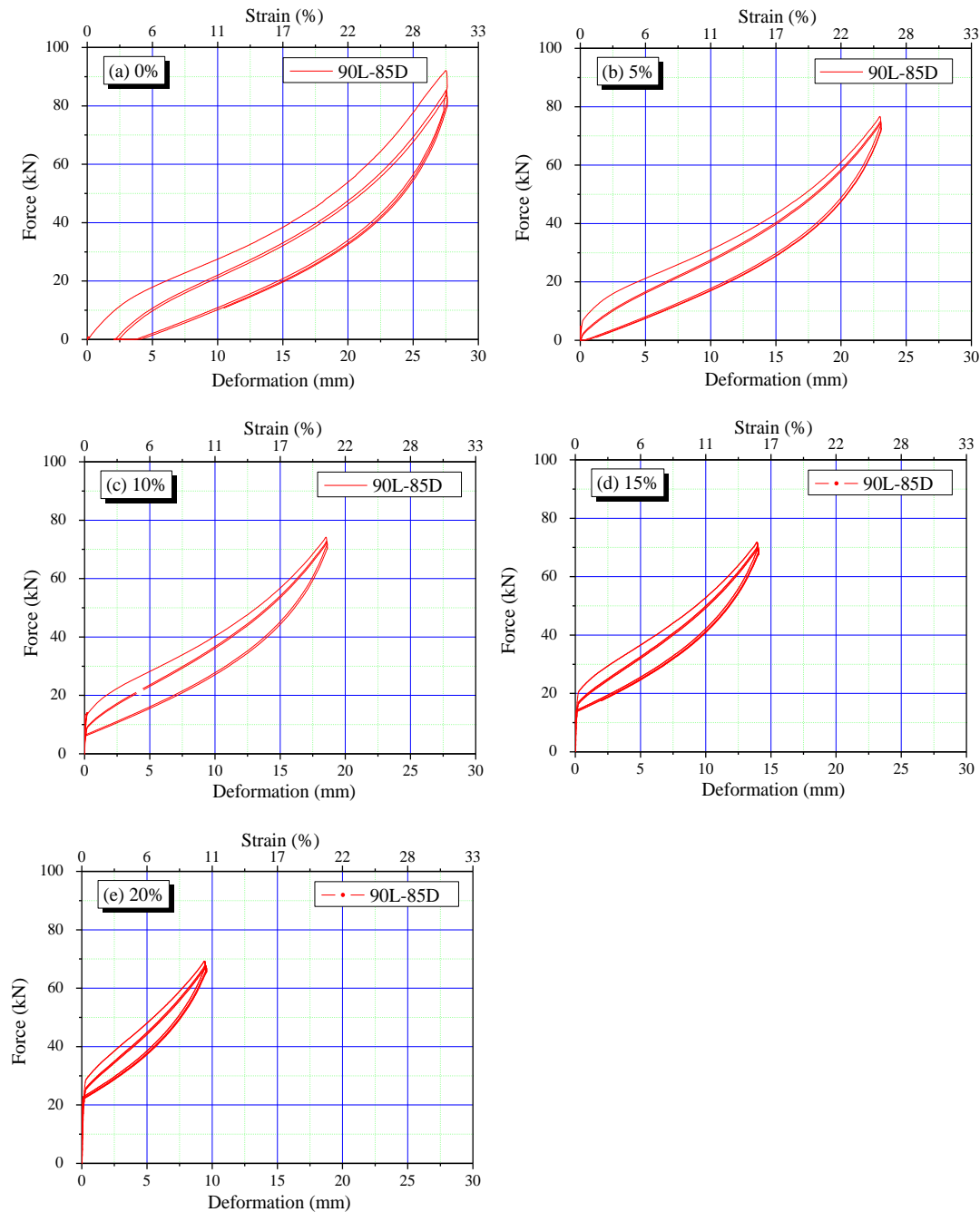
Fig. 4 Hysteretic curves of the 90L-85D specimen in Suite-II

4. Test results and discussion

In the compressive tests, each specimen produced five hysteretic force-deformation curves. This study shows the graphs of the smallest (80L-55D in Suite-I) and largest (100L-100D in Suite-III) specimens, as well as the middle one among them (90L-85D in Suite-II). Figs. 3-5 show the related curves. The three rubber spring specimens showed a similar behavior without precompression as well as under precompression. The other specimens except the three specimens also showed similar behavior, and they were consequently not included in this paper.

4.1 Compressive behavior without precompression

Typical compressive behavior of the polyurethane rubber springs followed softening and sequential hardening in the range of 30% strain. The softening occurred at 2-3% strain, and the hardening was observed at a strain of 15-17%. Strength degradation occurred from the second loading cycle, while the next cyclic loadings after the first cycle showed almost similar loading and unloading paths; thus, the rubber springs would be stabilized after the first loading cycle. The rubber springs in each suite were designed to have identical compressive stiffness; therefore,
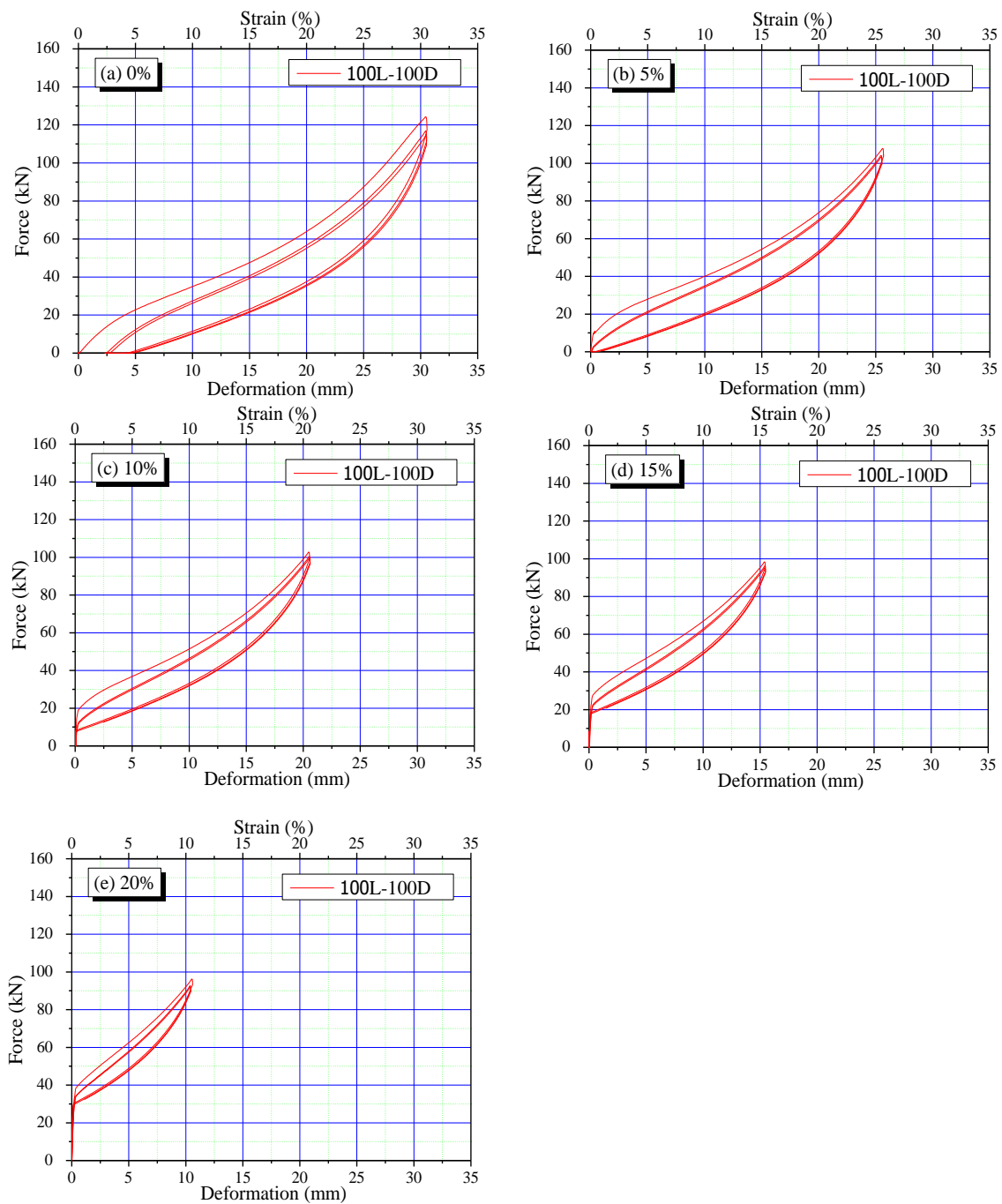
Fig. 5 Hysteretic curves of the 100L-100D specimen in Suite-III

it is expected that the three rubber springs in a suite would show an identical force-deformation curve in compression. Fig. 6 compares the first and second cyclic behavior of the three rubber springs in a suite. Except for the 80L-55D spring in Suite-I, the three rubber springs in each suite showed a similar loading path in the first and second cycles. The unloading path depends on the damping of the rubber springs and thus, they showed a little deviation. The 80L-55D rubber spring was manufactured previously, and it was not from the same bulk. This particular spring seems to produce a different loading path. The result in Fig. 6 shows

that the design procedure of the rubber springs worked well to induce identical compressive stiffness in the rubber springs. Therefore, the longer rubber springs in a suite can absorb more deformation with the same stiffness.

Unloading and residual deformations

The first loading cycle left deformation after unloading, and this is called unloading deformation or strain in this study. Its part was recovered immediately while the remaining part was not recovered, which was called residual deformation or strain (see Fig. 7(a)). Thus, the
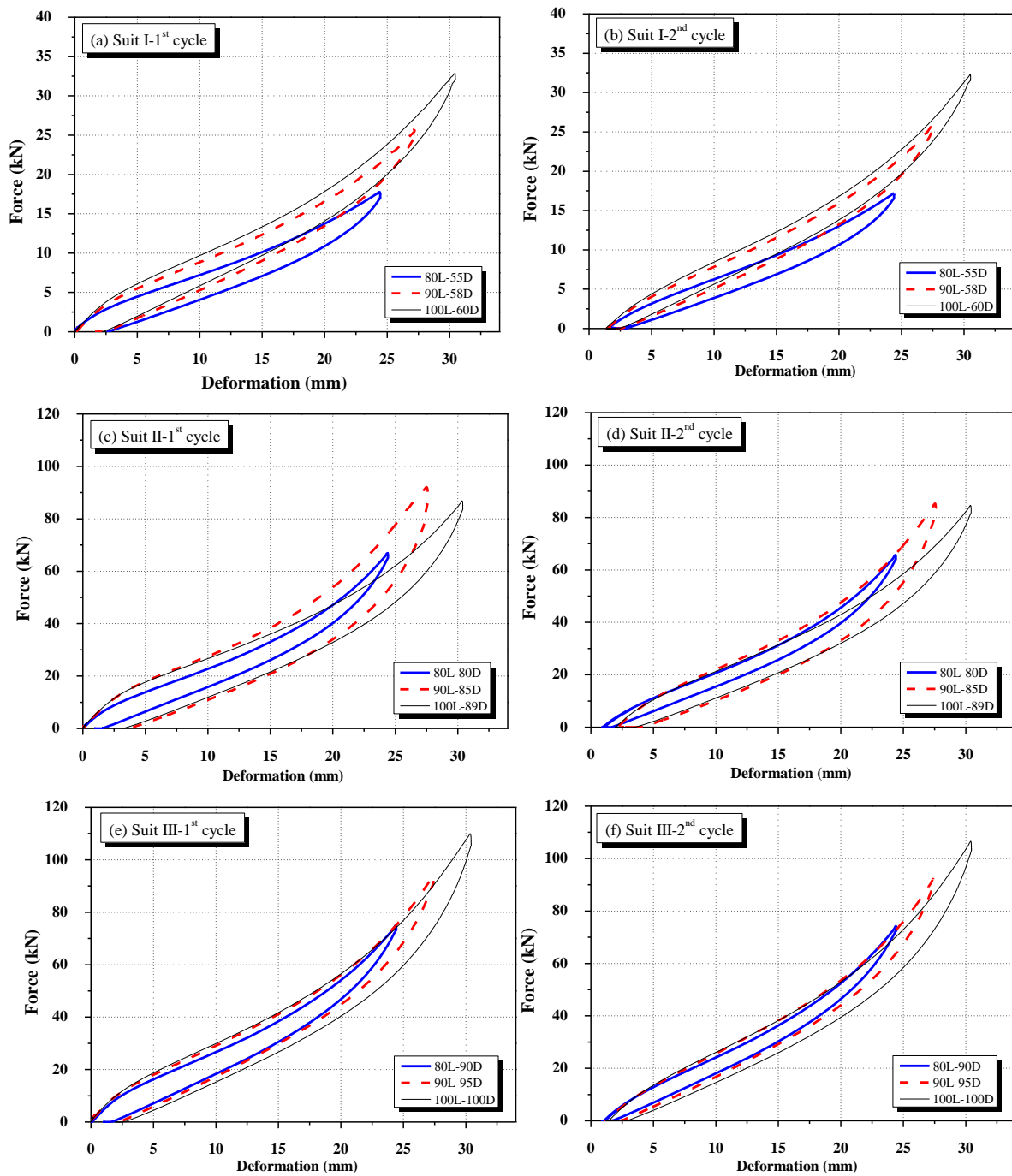
Fig. 6 Comparison of hysteretic curves of rubber springs in each suite

second loading started from the residual deformation and showed smaller strength than that of the first cycle. However, the unloading path of the second cycle followed the same path of the first cycle (see Figs. 3(a), 4(a) and 5(a)). This study conducted additional compressive tests of rubber springs without precompression with varying strain that was begun at 5% strain, increased by 5% up to 30% strain. For this, three rubber springs with 100 mm length, namely, 100L-60D, 100L-89D, and 100L-100D springs, were used, and Fig. 8 shows their hysteretic behaviors. Fig. 9 illustrates the unloading ε_{UL}, recovered ε_{RC}, and residual

strains ε_{RD} according to the loading strain. The unloading strain increased with increasing maximum loading strain.

The three rubber springs showed similar unloading strains up to 10% strain, while the 100L-60D rubber spring showed the smallest unloading strains after 10% strain. After recovering strain, the 100L-60D rubber spring retained the smallest residual strain after 10% strain. However, the other two rubber springs showed similar residual strains. Fig. 10 compares the ratios of unloading strain to loading strain and residual strain to unloading

(a) Without precompression
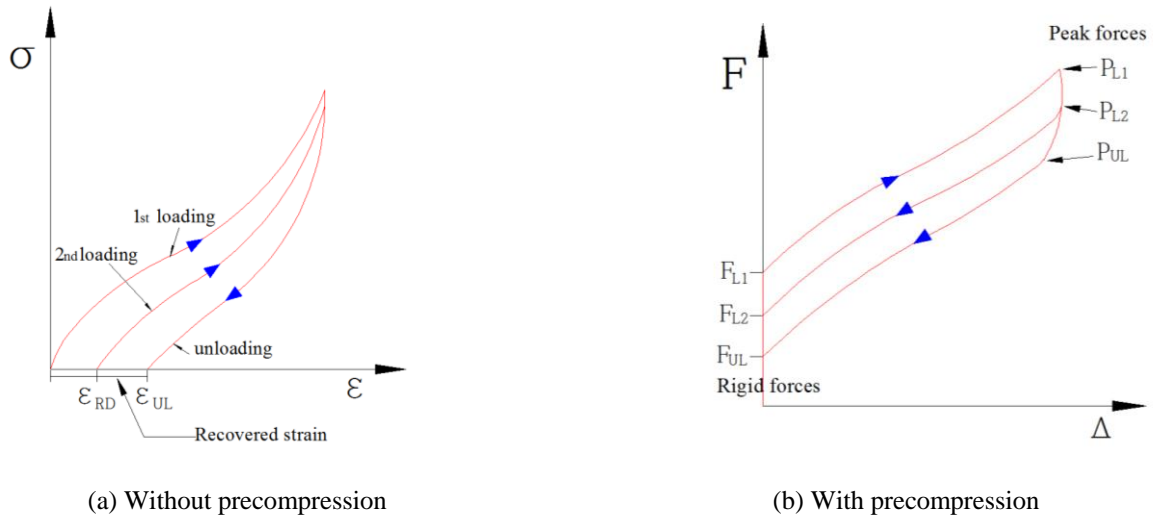
(b) With precompression

Fig. 7 Schematic drawing of hysteretic behavior of polyurethane rubber springs without and with precompression
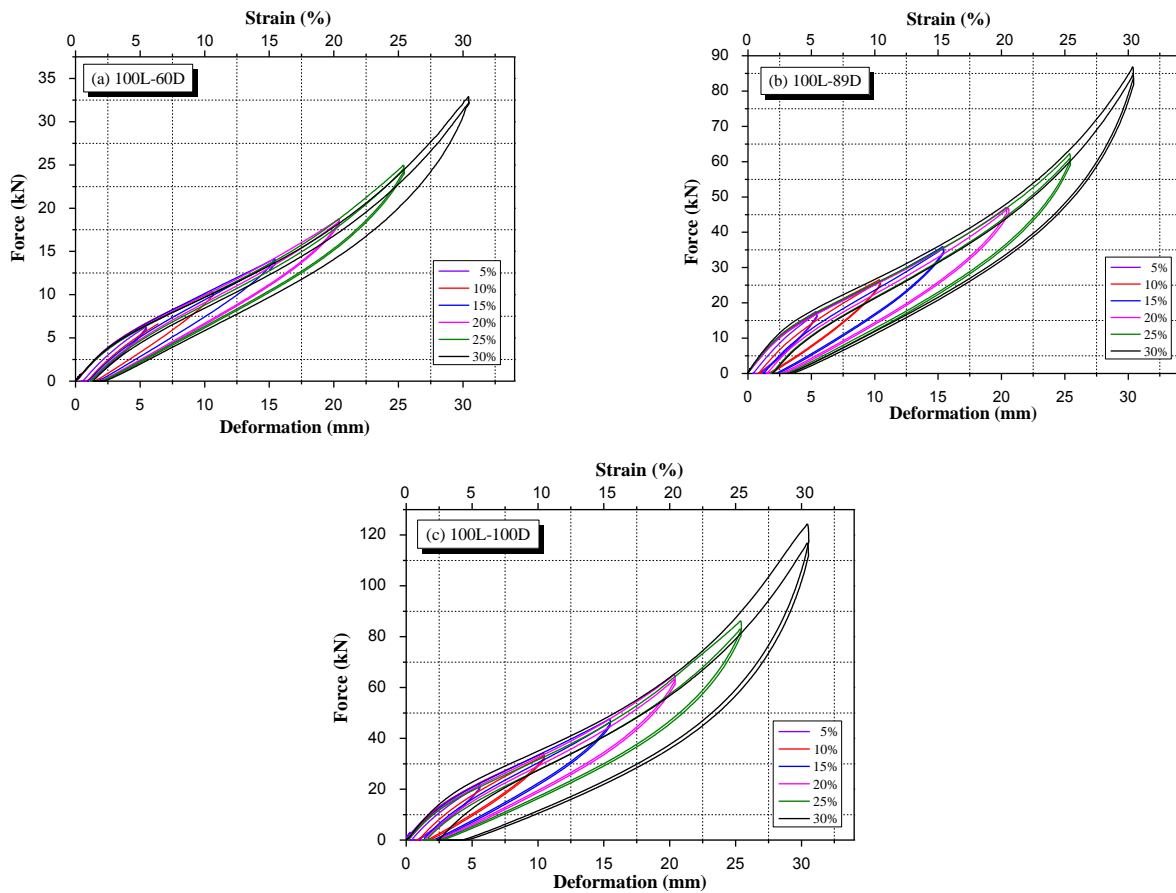

Fig. 8 Hysteretic behavior of rubber springs with varying compressive strain

strain. The unloading strain ratios decrease with increasing loading strain, and they showed a second order polynomial relationship. The residual strain ratios are almost stable regardless to loading strain; exceptionally, the 100L-89D spring showed an increasing trend. Average residual strain ratios of the 100L-60D and -100D springs were 57.6% and 67.6%, respectively. Fig. 11 shows the unloading and

residual strains of the nine rubber springs due to the loading of the 30% strain.

In Fig. 9, the smaller stiffness of rubber springs with an identical length showed the smaller unloading strain. However, this was not maintained in Fig. 11, where the 80L-50D spring showed the largest unloading strain although the spring possessed the smallest stiffness among
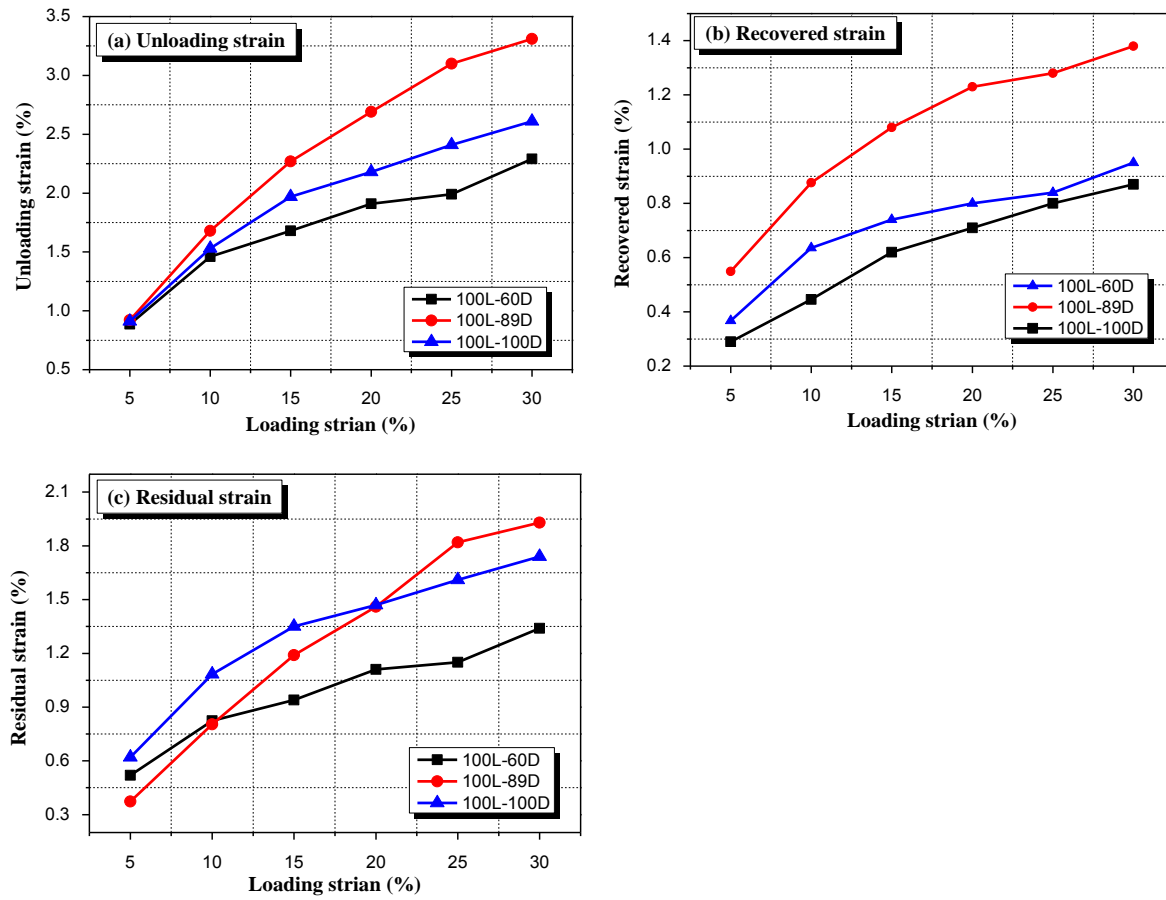
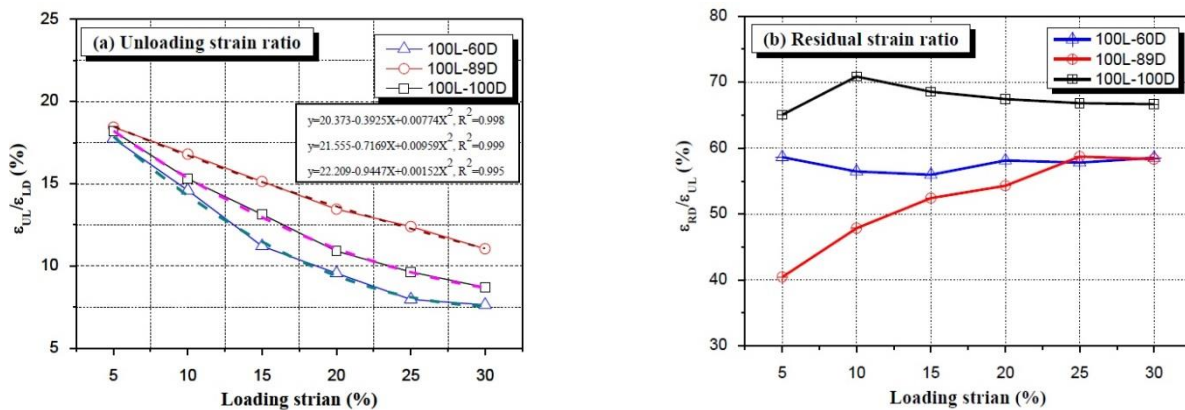Fig. 9 Unloading, recovered, and residual strains of rubber springs

Fig. 10 Unloading and residual strain ratios

the three springs with 80 mm length. Although there was a little deviation, in general, longer springs in a suite produced larger unloading and residual strains. The unloading strain ratios were also larger for longer springs while the residual strain ratios were stable; their average was 55.5%. Consequently, more than half of the unloading strain remained as residual strain.

Stiffness variation

As shown in Fig. 8, polyurethane rubber springs showed a highly nonlinear behavior; they showed variation of stiffness according to applied loading strain. This study estimated effective stiffness from the loading path to investigate stiffness variation with increasing loading strain.
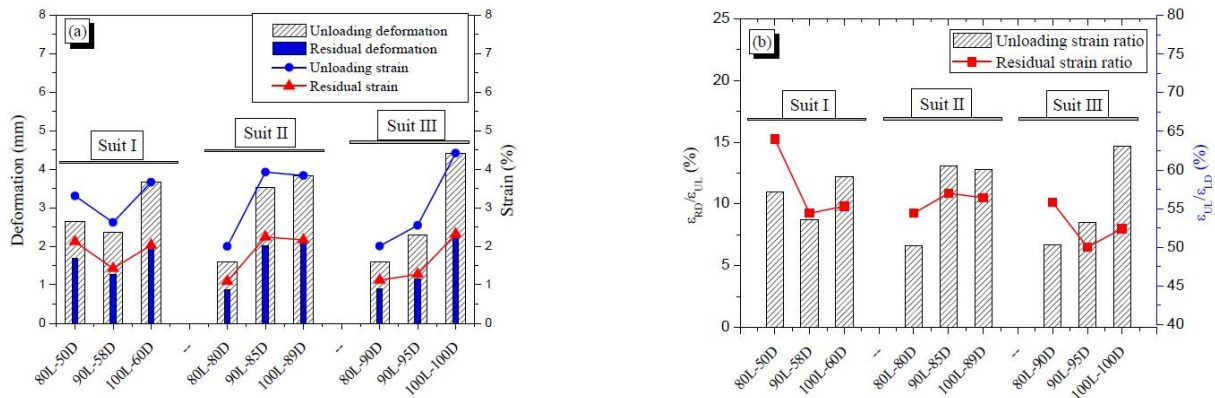
Fig. 11 Unloading and residual strains due to 30% loading strain of nine rubber springs
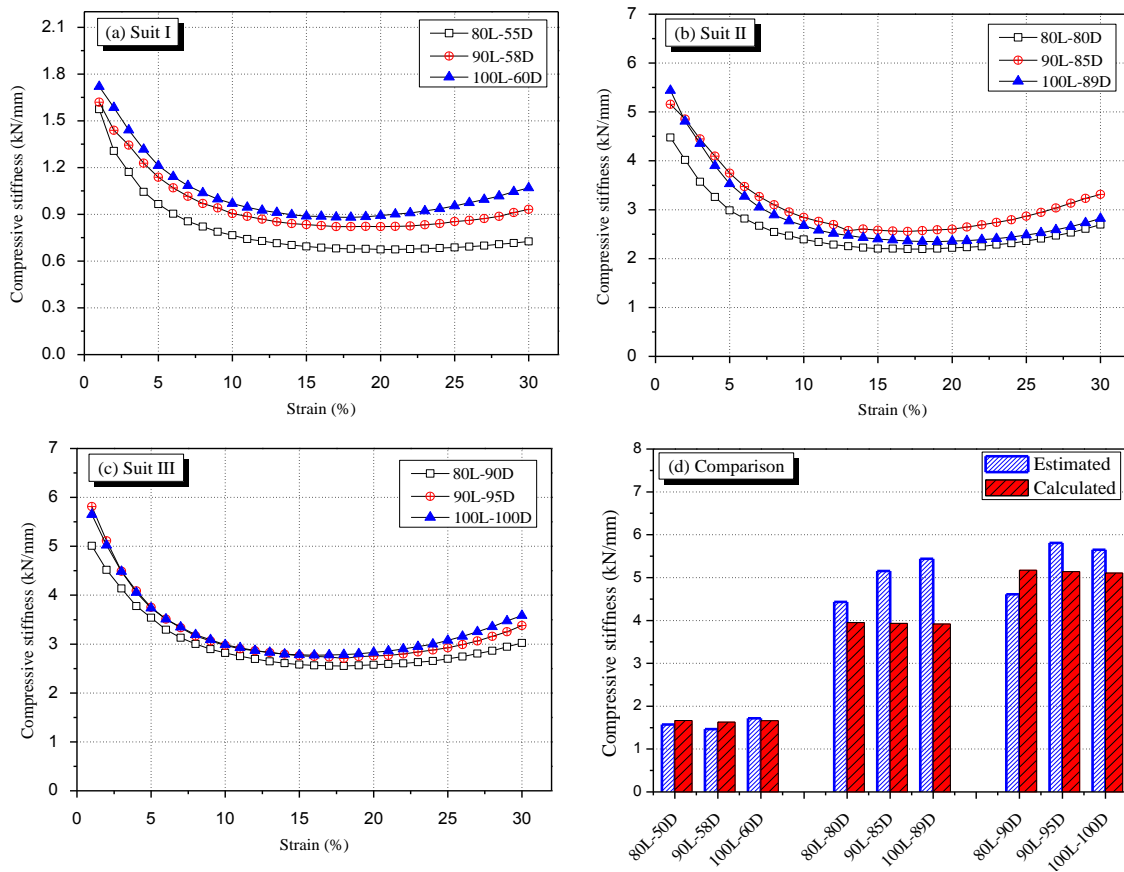

Fig. 12 Measured compressive stiffness of rubber springs and comparison with the calculated stiffness

The effective stiffness was calculated as the slope from the origin to the point of the applied force for a specific strain or deformation. Fig. 12 shows the stiffness variation of rubber springs in the three suites according to the applied loading strain. The effective stiffness was estimated from 1% to 30% strain with increasing 1% strain. For Suite-I that possessed relatively low stiffness, the shorter spring showed lower stiffness. However, this trend gradually disappeared with increasing stiffness for a suite. The maximum strain, which occurred at the strain of 1%, generally became larger

with the longer spring; however, the maximum stiffness of the 90L-95D spring in Suite-III was larger than that of the 100L-100D spring. This result indicated that the length of the rubber springs in a suite has less effect on stiffness variation if the stiffness of the rubber springs became relatively large.

The compressive stiffness for all the rubber springs initially reached the maximum and decreased up to strain of approximately 15% strain. After that, the stiffness hardening was observed up to 30% strain. The maximum

Table 2 Maximum and minimum estimated effective stiffness of rubber spring

Suite	Specimen	k_c (kN/mm)	$k_{E\text{-max}}$ (kN/mm)	k_{E-max}/k_c (%)	$k_{E\text{-min}}$ (kN/mm)	ϵ_{E-min} (%)	k_{E-min}/k_{E-max} (%)
Suite- I	80L-55D	1.665	1.575	94.6	0.6750	20.0	42.9
	90L-58D	1.629	1.62	99.5	0.8211	20.0	50.7
	100L-60D	1.661	1.72	103.6	0.8811	18.0	51.2
	Average	1.652	1.638	99.2	0.79	19.3	48.26
Suite- II	80L-80D	3.951	4.435	112.3	2.1949	17.0	49.5
	90L-85D	3.933	5.156	131.1	2.5569	17.0	49.6
	100L-89D	3.917	5.44	138.9	2.3474	18.0	43.2
	Average	3.933	5.010	127.4	2.37	17.3	47.41
Suite- III	80L-90D	5.172	5.010	96.9	2.5535	18.0	51.0
	90L-95D	5.138	5.811	113.1	2.7074	18.0	46.6
	100L-100D	5.109	5.650	110.6	2.7744	16.0	49.1
	Average	5.140	5.490	106.8	2.68	17.3	48.89

stiffness for all rubber springs was measured at 1.0% strain (see Table 2), and they were compared with the calculated stiffness using Equation (3) in Table 1 (see Fig. 12(d)). For Suite-I, the calculated stiffnesses of the springs were close to the maximum estimated stiffness; two springs showed higher and the other one showed smaller stiffness, with a calculated average difference reaching only 0.8%. However, for Suite-II, three estimated stiffnesses were greater than the calculated stiffnesses; the average difference was 21.5%. For Suite-III, one spring produced an estimated stiffness that was very close to the calculated one. However, the other two springs showed relatively large deviation; the average difference was 6.4%. For Suite-I, the calculated stiffness was matched with the estimated stiffness at around 1% strain. For Suite-III, the corresponding strains occurred at approximately 2% strain. However, for Suite-II, the corresponding strains varied from 2% to 4% strain.

The springs generally are used for dampers, and deformation as large as possible is necessary to absorb the large displacement of the damper. If the possible maximum strain is 30%, the allowable strain could be below that. In that case, the maximum stiffness at 1.0% strain cannot represent the behavior of the rubber springs. Table 2 shows the minimum stiffness of the springs with the corresponding strains. The minimum stiffness occurred at the strain ranging from 16% to 20%; the corresponding strains for Suite-I was close to 20%, and those for Suite-II and -III are close to 17%. The minimum estimated stiffness was approximately 48% of the maximum stiffness on average. Additionally, the estimated stiffness at 10% strain was less than 60% of the maximum stiffness for all of the springs. From experience, for application, the required deformation of the springs should exceed 10% strain. Therefore, considering the range of applied deformation of the springs, the designed stiffness of the springs should be conservatively half of the maximum stiffness of 1% strain. If experimental data is not available, the calculated stiffness would be used instead of the experimental maximum stiffness.

Damping ratio

Damping ratios ξ using Eq. (4) due to 30% strain loading for the nine springs were estimated, and damping ratios of three springs with 100 mm length were also estimated with variation of loading strain using the hysteretic curves in Fig. 8.

$$\xi = \frac{1}{4\pi} \frac{E_D}{E_S} \tag{4}$$

where, E_D and E_S are dissipated and elastic energy for a hysteretic curve.

As shown in Fig. 13(a) (also see the third column in Table 3), the springs in Suite-I, which had relatively low stiffness, showed the largest average damping ratio of 2.62%, and they showed similar damping ratios. The average damping ratio decreases with increasing stiffness; thus, the springs in Suite-III showed the smallest average damping ratio of 2.09%. In Suite-II and -III, the shortest springs showed the smallest damping ratios. In a suite, longer springs generally produced larger damping ratios.

The damping ratio affects the unloading strain, and a larger damping ratio generally induced larger unloading strain. For the 100L-100D spring, its damping ratio was 2.91%, and that was the largest among all the springs, Its unloading and residual strains were 4.41% and 2.31%, respectively, which were also the greatest. Fig. 13(b) shows the variation of damping ratio according to loading strain for the three springs of 100L-60D, -89D, and -100D. The damping ratio decreased with increasing loading strain; the damping ratios at 30% strain for the 100L-60D and -89D springs were 47.4% and 61.8% of the damping ratios at 5% strain, respectively. The only exception occurred at 30% strain of the 100L-100D spring.

The damping ratio at 30% strain of the 100L-100D spring in Fig. 13(b) was 2.92, and that was larger than the damping ratio of 2.46 at 25% loading strain.

For the cases of 30% loading strain, the 100L-60D and -89D springs showed different damping ratios in Figs. 13(a) and 13(b) while the 100L-100D spring showed almost the same damping ratio for the two tests; for the 100L-60D and -89D springs, the damping ratios at 30% strain in Figure 13b were 65.6% and 82.8% of the corresponding values in Fig. 13(a), respectively. The springs used for Fig. 13(b) were tested continuously with increasing loading strain and with a short rest between tests, while the springs used for
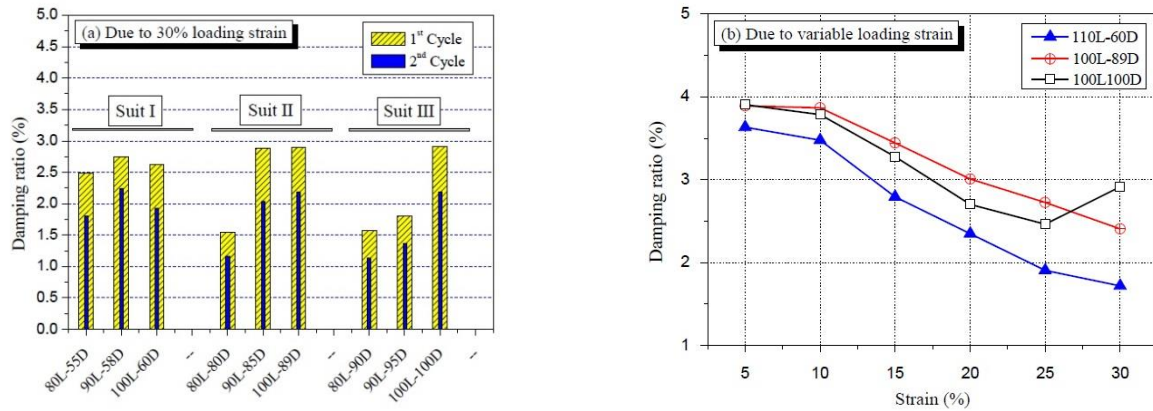
Fig. 13 Comparison of damping ratio of rubber springs without precompression

Table 3 Damping ratios of rubber springs with precompression

Suite	specimen	0%	5%	10%	15%	20%
Suite- I	80L-55D	2.49	2.50	2.64	2.65	2.70
	90L-58D	2.75	2.80	3.09	3.18	3.75
	100L-60D	2.62	2.45	2.53	2.61	2.79
	Average	2.62	2.58	2.75	2.81	3.08
Suite- II	80L-80D	1.55	1.57	1.62	1.72	1.74
	90L-85D	2.88	2.54	2.59	2.59	2.59
	100L-89D	2.90	2.62	2.62	2.70	2.72
	Average	2.44	2.24	2.28	2.34	2.35
Suite- III	80L-90D	1.57	1.54	1.61	1.65	1.69
	90L-95D	1.80	1.79	1.83	1.84	1.67
	100L-100D	2.91	2.70	2.74	2.75	2.70
	Average	2.09	2.01	2.06	2.08	2.02

Fig. 13(a) were applied directly up to 30% strain first of all. Thus, it appears that the hysteresis of the rubber spring was affected by its loading history and stiffness.

In Fig. 13(b), the shortest spring of 100L-60D among the three springs showed the smallest damping ratios over all ranges. In Fig. 13(a), the 100L-60D spring showed a damping ratio of 2.62 that was larger than the corresponding values of the 100L-89D and -100D springs; thus, the result in Fig. 13(b) can be reliable. However, for the springs with 80 mm length in Fig. 13(a), the 80L-55D showed the largest damping ratio of 2.44 compared with the other two damping ratios of 1.55 and 1.57. For the springs of middle length at 90 mm, the 90L-95D spring showed the smallest damping ratio while it had the largest stiffness among them. Variation of the damping ratio therefore seems to depend on the stiffness and length of the springs. Fig. 13(a) also shows the damping ratios of hysteretic curves of the second cycle. Their values were only 70-80% of their corresponding values of the first cycle. Thus, the second cycle damping ratios should be used for designing a damper.

4.2 Compressive behavior under precompression

Precompression

Precompression of the rubber springs is considered to remove the unrecovered deformation after unloading and to introduce a rigid force for self-centering. The rubber springs, after unloading, displayed an unloading strain, and part of this was immediately recovered. Thus, to remove a region of zero-force, the strain of precompression should exceed the unloading strain. The maximum unloading strain of 4.41% occurred for the 100L-100D spring (see Fig. 11(a)). If the above expectation worked well, the spring would not show a zero-force region with a precompression of 5% strain. However, the spring still showed a zero-force region of about 0.45% strain. When the unloading strain was 3.83% for the 100L-89D spring, the zero-force region disappeared with the precompression of 5% strain. Therefore, it was found that the strain of precompression should be larger than the unloading strain to perfectly remove the zero-force region.

This study used regression to determine the required minimum strain of precompression to eliminate the zero-force region. For this, the unloading rigid forces F_{UL} were estimated for the nine rubber springs (see Fig. 7(b)); if the
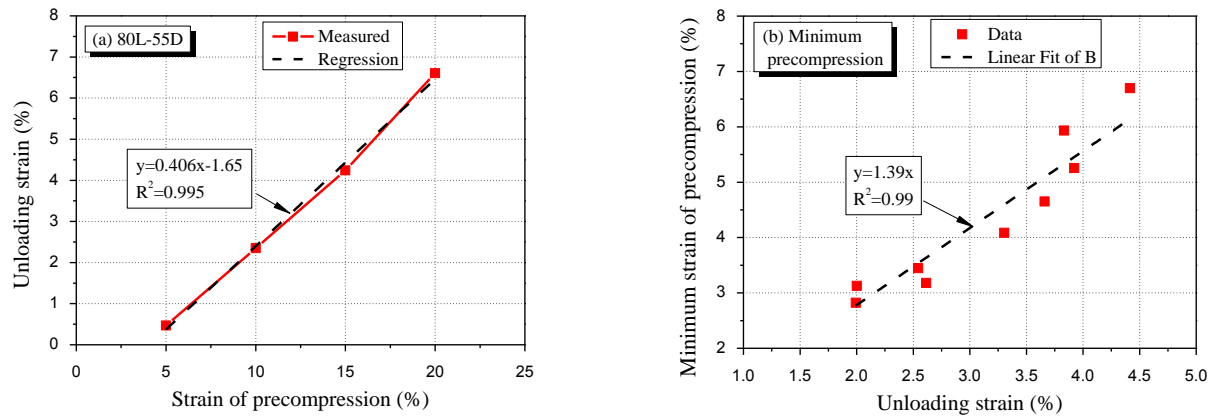
Fig. 14 Regression to determine the minimum strain of precompressio

Table 4 Results of regression to estimated minimum required strain of precompression

Suite	Specimen	Slop (a)	Const. (b)	R^2	x-intercept (%)	Unloading strain (%)
Suite- I	80L-55D	0.4061	-1.6589	0.997	4.085	3.304
	90L-58D	0.6234	-1.9819	0.9989	3.179	2.615
	100L-60D	0.7364	-3.4245	0.9974	4.650	3.661
Suite- II	80L-80D	1.4414	-4.0653	0.9976	2.820	1.994
	90L-85D	1.6233	-9.8788	0.9999	6.086	3.922
	100L-89D	1.8372	-10.896	0.9988	5.931	3.833
Suite- III	80L-90D	1.8385	-5.749	0.9997	3.344	2.002
	90L-95D	2.017	-6.949	0.9982	5.397	2.544
	100L-100D	2.22	-14.868	0.999	7.353	4.415

unloading rigid force was zero, the force was excluded from regression since the point disturbed the regression result. The unloading rigid force showed a linear relationship with a precompression strain. Table 4 shows the results of regression and Fig. 14(a) shows an example of the regression for the 80L-55D spring. Their relationship can be expressed with a linear equation (y=ax+b), and the x-axis intercept of (-b/a) from the regression equation indicates the minimum precompression strain to eliminate the zero-force region. The relationship between the minimum precompression strain and unloading strain after the loading 30% strain is shown in Fig. 14(b). The two data showed a linear relation with a slope of 1.39. This indicates that the minimum required strain of precompression should be 39% larger than the unloading strain of 30% loading to eliminate the zero-force region. The minimum required precompression strain may not significantly relate to the stiffness of the rubber spring, while longer rubber springs require more precompression to eliminate the zero-force region; the average values of the 80L-, 90L-, and 100L-springs are 3.344, 4.237, and 5.759%, respectively.

Rigid force
As shown in Figs. 3-5, the behavior of the precompressed rubber springs with a sufficient pre-compression initially showed rigid force and subsequent hysteretic curves. However, as shown in Fig. 15, the first

loading path with precompression did not reach the loading path without precompression; there was strength degradation due to precompression. In addition, the second loading path with precompression also did not reach the first loading path; Fig. 15 shows hysteretic curves with and without precompression, and F_{IL} indicates the initial loading force without precompression, and F_{L1} and F_{L2} represent the rigid forces due to precompression in the first and second cycles. Thus, this study analyzed the rigid forces of the first and the second loading cycles, respectively.

The rigid forces of F_{L1} and F_{L2} show an almost linear relationship to the strain of precompression (see Fig. 16), and their result of regression is illustrated in Table 5. Several observations were found related to the rigid force:

• The rigid forces of F_{L1} and F_{L2} increased with increasing precompressive strain.

• The slopes of regression increased with larger stiffness of rubber springs.

• The rigid forces of the rubber springs in Suite-I and -II became greater with longer length rubber springs, while this trend disappeared for the springs in Suite-III.

• Also, the springs in Suite-III showed similar rigid forces even with different lengths, and the gaps between rigid forces at the same strain decreased with higher stiffness of rubber spring.
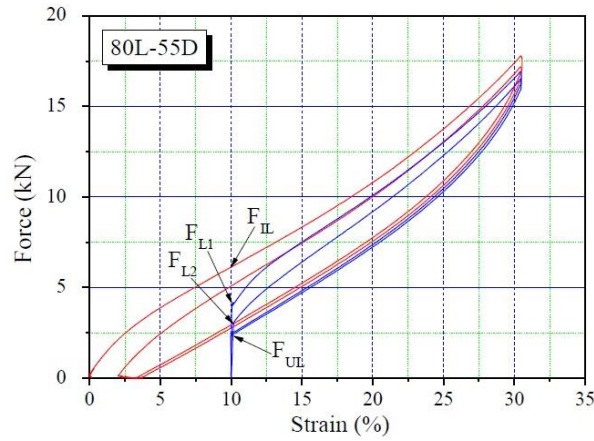
Fig. 15 Hysteretic curves of the first cycle with and without precompression
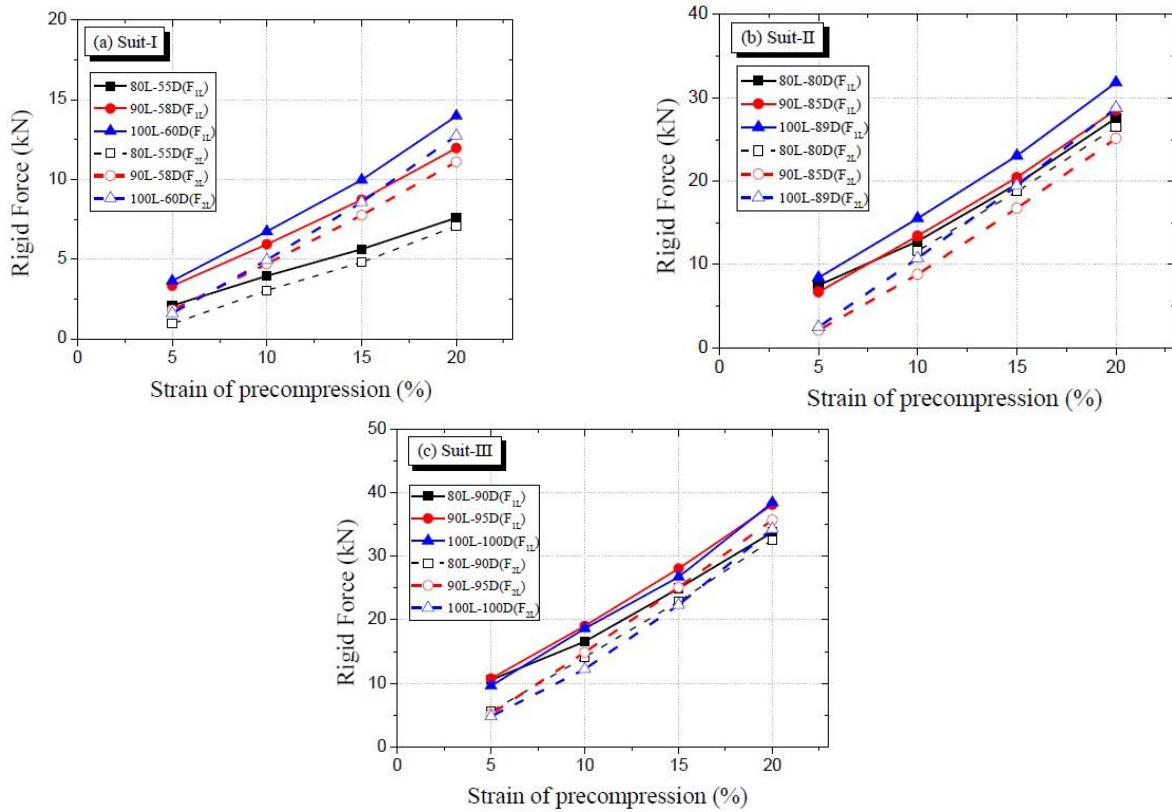

Fig. 16 Rigid forces of rubber springs due to precompression

• Thus, it seems that the length of rubber springs with relatively low stiffness has significant effect on the two kinds of rigid forces.

This study also analyzed the difference between F_{IL} and F_{L1}, $\Delta(F_{IL} - F_{L1})$, and the difference between F_{L1} and F_{L2}, $\Delta(F_{L1} - F_{L2})$. $\Delta(F_{IL} - F_{L1})$ indicates the strength reduction from initial loading without

precompression to the first loading with precompression, and $\Delta(F_{L1} - F_{L2})$ represents the reduction from the first to the second loading under precompression. As shown in Fig. 17, the springs in Suite-I showed a smaller reduction of $\Delta(F_{IL} - F_{L1})$ compared with the springs in Suite-II and – III; thus, it was found that the rubber springs with lower stiffness showed smaller strength reduction due to the precompression. The reduction of $\Delta(F_{IL} - F_{L1})$ generally increased with longer springs in a suite and larger strain of

(a) Difference of $\Delta(F_{IL} - F_{L1})$

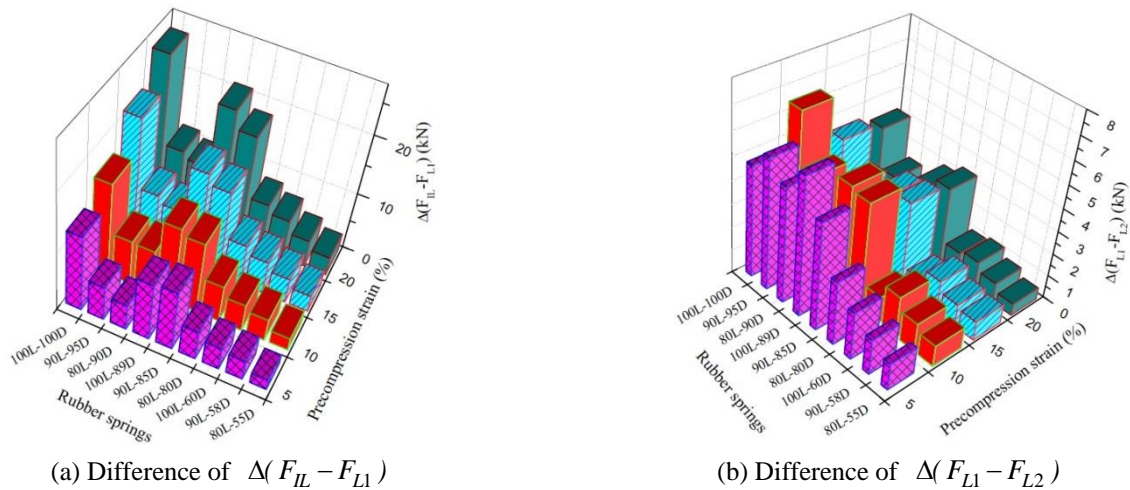(b) Difference of $\Delta(F_{L1} - F_{L2})$

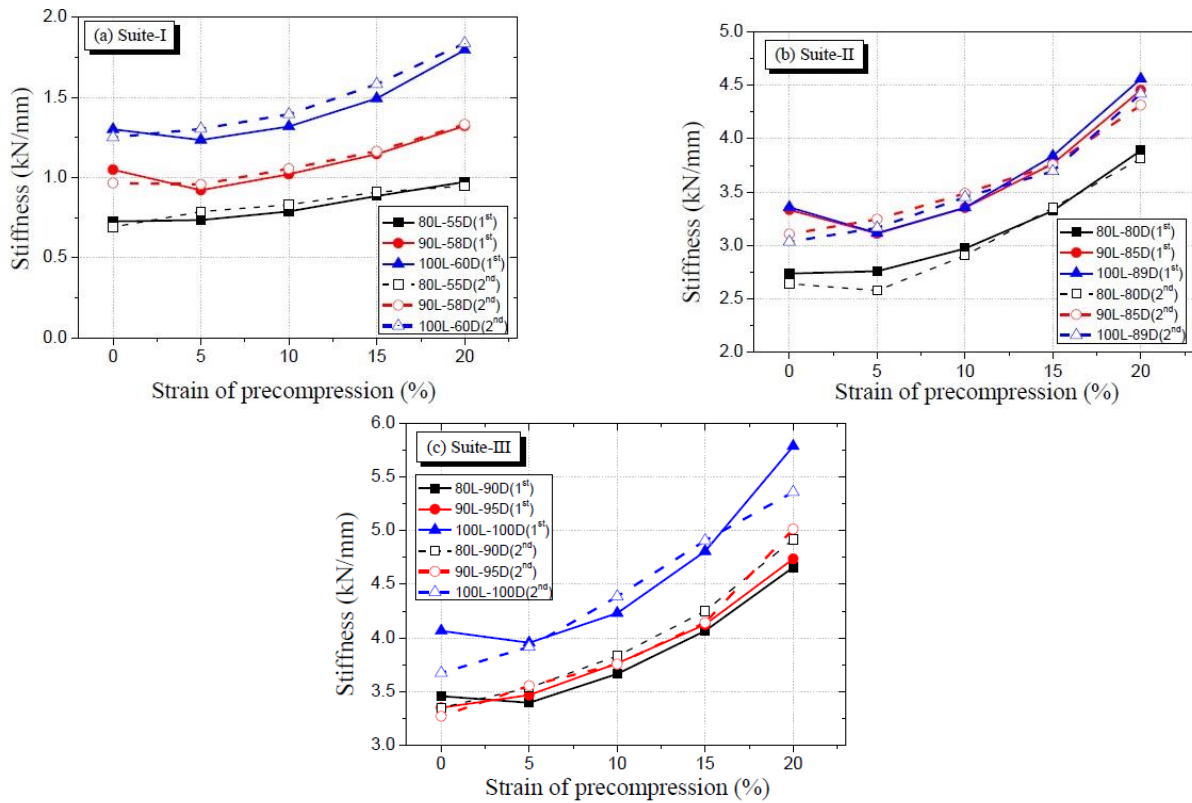Fig. 17 Strength degradation of rigid forces

Fig. 18 Effective stiffness of precompressed springs according to precompressive strain

precompression. The reduction of $\Delta(F_{L1} - F_{L2})$ showed larger values with smaller precompressive strain, and it increased with longer springs. The springs in Suite-I also showed a smaller reduction of $\Delta(F_{L1} - F_{L2})$ compared with the springs of Suite-II and –III. It is conjectured that the first reduction of $\Delta(F_{IL} - F_{L1})$ was greater with larger strain and, thus, the second reduction of $\Delta(F_{L1} - F_{L2})$ became smaller even with the larger strain of precompression.

Stiffness variation

For precompressed rubber springs, the compressive behavior consisted of a rigid part and hysteresis. This study estimated the effective stiffness of hysteretic curves between the rigid force and peak force; thus, the rigid part was excluded in the estimation. The total compressive strain of the rubber springs with precompression was identical at 30%. In Fig. 18, zero strain in the x-axis indicates the stiffness without precompression when a rubber spring was compressed with 30% strain.

Table 5 Results of regression of rigid forces

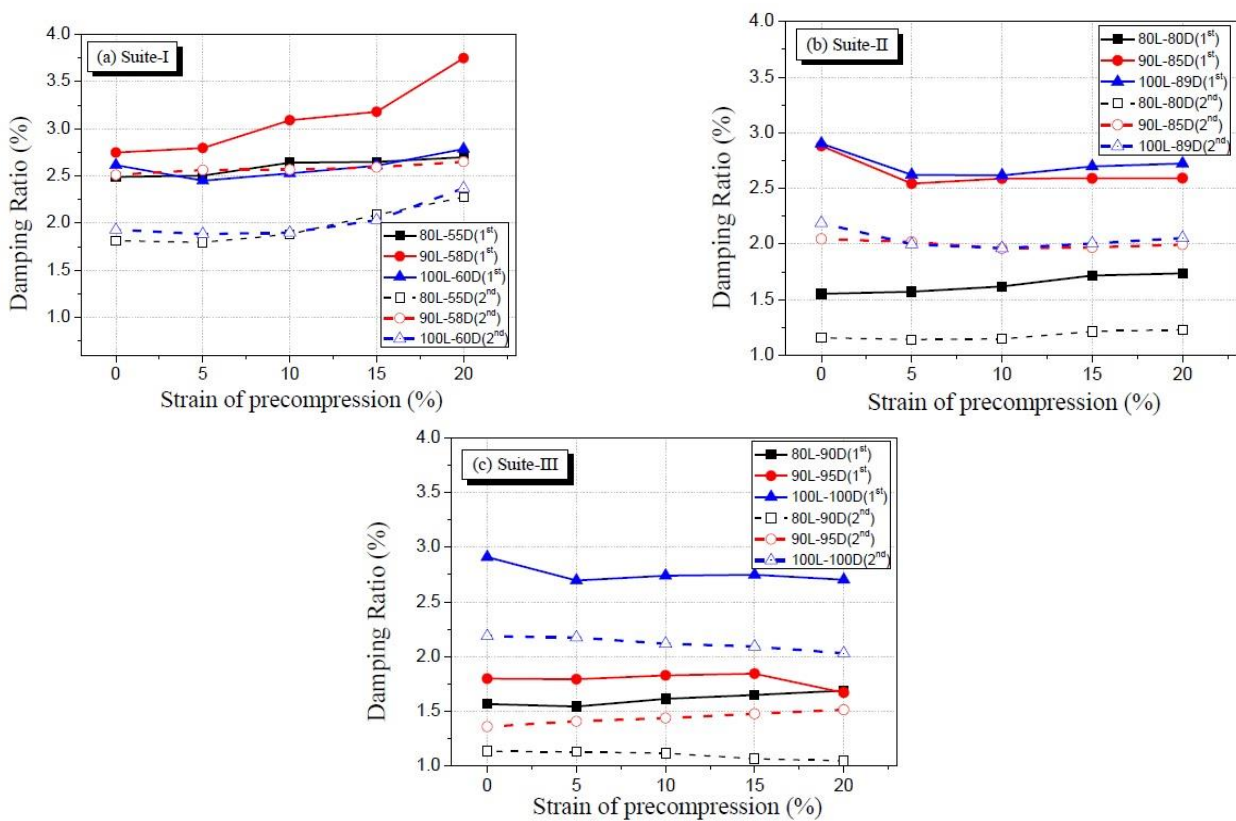| Suite	Specimen	Slop	Const.	R^2
	80L-55D	0.3631	0.2749	0.9991
Suite- I	90L-58D	0.5737	0.3081	0.9976
	100L-60D	0.6851	0.0125	0.9962
	80L-80D	1.3412	0.1068	0.9922
Suite- II	90L-85D	1.4515	-0.861	0.9981
	100L-89D	1.5561	0.247	0.9976
	80L-90D	1.5595	1.9733	0.9931
Suite- III	90L-95D	1.82	1.243	0.9982
	100L-100D	1.5595	1.9733	0.9931

Fig. 19 Damping ratios of precompressed springs according to precompressive strain

The stiffnesses from the first loadings were similar to those of the second loadings regardless of the designed stiffness and length. The stiffness of the precompressed springs increased monotonically with increasing precompressive strain; the linear relationship for Suite-I was relatively high, but it diminished for Suite-II and -III. Therefore, the linearity between the stiffness and precompression decreased with increasing the designed stiffness of the rubber springs. Also, the stiffnesses at 5% strain precompression were similar to or a little lower than those of springs without precompression. However, the stiffnesses beyond 5% strain precompression were greater than those at the zero strain of precompression. In a suite of springs, longer springs generally had greater stiffness; In Suite-I, the stiffness increased by approximately 30% with increasing length by 10 mm. However, for Suite-II, the

80L-80D and 90L-85D springs showed an almost similar variation of stiffness, and, for Suite-III, the 80L-90D and 90L-95D springs showed a similar trend of stiffness. The estimated stiffness of the precompressed springs would be helpful in developing an analytical model by compounding the rigid force.

Damping ratio

The damping ratio of the precompressed rubber springs was estimated using Eq. (4). The rigid part of the behavior was not included to calculate elastic energy E_S, and thus, the damping ratio was estimated only considering the hysteretic part. The precompressed rubber springs showed an almost stable damping ratio regardless of precompressive strain from 5% to 20% strain, except for the 90L-58D spring that showed increasing damping ratio with
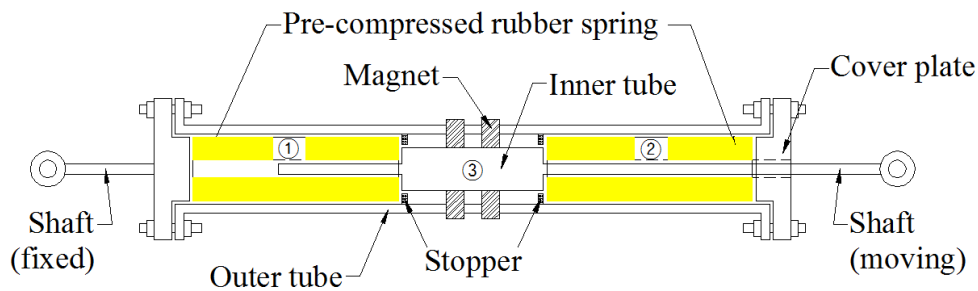
Fig. 20 Schematic drawing of self-centering device using pre-compressed rubber springs (Choi *et al*. 2017)

increasing precompression (see Fig. 19). Based on the first loading cycle, the maximum average damping ratio of the precompressed rubber springs was 3.20% of the 90L-85D spring, and the minimum value occurred in the 80L-90D spring at 1.62%. These average values generally were close to or smaller than the corresponding damping ratios of the unprecompressed rubber springs with loading of 30% strain. The springs in a suite showed deviation of the damping ratio. It appears that the damping ratio of the precompressed rubber springs is not highly related to the stiffness or length of the springs.

The second loading cycles showed a reduction in damping ratio because of strength degradation in the rigid force. The reduction ratio was largest for the 80L-90D spring by 33% and smallest for the 90L-95D by 18%. The damping ratio was almost stable with increasing precompression, while the 80L-55D and 100L-60D springs in Suite-I showed a small increment with increasing precompression.

5. Discussions

The polyurethane rubber springs showed the unloading paths deviated from the loading paths because of viscosity and residual deformation due to unloading. The residual deformation with zero-force should be removed for the self-centering capacity of the rubber spring, and the precompression was proved to be an effective solution to eliminate the residual deformation as well as to provide rigid force. The precompressed rubber springs showed strength degradation, and the extent of the degradation became severe with larger precompression. This is something that should be considered when designing rubber springs with precompression. The damping ratio of the rubber springs without precompression was below 4% with a relatively small compressive strain of 5%, and the value became smaller with increasing compressive strain. The precompressed rubber springs also showed below a 4% damping ratio. Thus, rubber springs with and without precompression appear not to provide sufficient damping ratio, and an additional damping device should therefore be used in parallel to obtain more than a 10% damping ratio. A previous study obtained a 7% damping ratio by combining precompressed rubber springs and the friction of magnets.

The calculated stiffness of the rubber springs using Eq. (3) was matched with the stiffness at a small compressive strain of 1%. The rubber springs are expected to operate at over 10% strain, and the stiffness of the rubber springs thus became almost half of a calculated one. To obtain a stiffen spring, rubber springs can be arranged in parallel. Moreover, to face a long deformation, a serial combination of the rubber springs could be used; a rubber spring with too long a length may not be used because of buckling and bulging.

The rubber springs that were designed to have an identical compressive stiffness showed similar loading and unloading paths, while they showed different behaviors of unloading residual strain, rigid forces, loading and unloading stiffness. As a result, it is recommended that a rubber spring be tested before application in a device.

The rubber springs with pre-compression can be used for a self-centering device as shown in Fig. 20 (Choi *et al*. 2017). In the figure, each rubber spring was activated in pulling or pushing action, and a pilot test of the device resulted in a flag-shaped behavior. In the device, additional damping using magnetic or mechanical friction can be obtained; thus, the device can provide sufficient energy dissipation capacity for seismic application (Jeong *et al*. 2016).

6. Conclusions

This study conducted compressive tests of rubber springs made of polyurethane rubber considering precompression. The rubber springs were manufactured in three suites of nine springs, and the rubber springs in a suite were designed to have an identical compressive stiffness even with different lengths. Therefore, this study considered the compressive stiffness, length, and precompressive strain of rubber springs for the tests, and several observations and findings were obtained. The rubber springs with sufficient precompression showed an initial rigid force and subsequent hysteretic behavior; thus, it was found that they can be applied to self-centering devices.

The rubber springs in a suite without precompression showed similar force-deformation curves regardless of different lengths, and thus Eq. (3) can be used to design various lengths of rubber springs with an identical compressive stiffness. The unloading and residual strains of the rubber springs without precompression increased with

increasing precompressive strain, and the residual strain ratio of the three springs varied approximately from 50% to 70%. With the precompression of 30% strain, the maximum unloading and residual strains were 4.4% and 2.3%, respectively. The effective compressive stiffness of the rubber springs without precompression decreased with increasing compressive strain up to 16-20% strain, and then stiffness hardening occurred. The minimum stiffness was approximately half of the stiffness at 1% strain; this should be considered for designing rubber springs. The calculated stiffnesses using Eq. (3) were close to those at small strains of 1-4%. The damping ratio of the rubber springs without precompression decreased with increasing compressive strain. For 5% strain, the maximum damping ratio did not exceed 4%, and, for 30% strain, the maximum damping ratio was 2.9%. Moreover, the damping ratio of the second hysteretic cycle was reduced approximately by 75% of the damping ratio for the first cycle. The minimum required precompressive strain to eliminate the unloading strain was estimated using linear regression based on the unloading strain due to the loading with 30% strain. The minimum precompression should be 40% larger than the remaining strain after unloading due to the loading of 30% strain, and this is very critical for the rubber spring to provide rigid force and self-centering capacity.

The loading rigid force due to precompression increased linearly by increasing the precompressive strain, and it did not reach the loading path without precompression; thus, there was strength degradation. The unloading rigid force was reduced from the loading one and also showed a linear relationship to the precompressive strain. When the minimum required precompression is applied on a rubber spring, the unloading rigid force is expected to be zero.

The loading stiffness of the precompressed rubber springs generally was greater than that of the rubber springs without precompression. The loading stiffness of the precompressed rubber springs also increased with increasing precompression because a larger precompression induced greater strength reduction from the loading path of the unprecompressed rubber springs, while the strength reduction at the peak point was relatively small. The loading stiffnesses of the second cycles almost coincided with those of the first cycles. The unloading stiffnesses of the precompressive rubber springs also showed similar values to those of the first and second cycles. Thus, they can be modeled in parallel for an analytical model.

For the first cycle, the damping ratios of the precompressed rubber springs were almost stable regardless of precompressive strain, and the shortest rubber spring in a suite showed the smallest damping ratio. For the second cycle, the damping ratio was reduced by 8% to 38% from that of the first cycle. The average reduction ratios were larger than 20% except for the two springs of 90L-58D and 90L-95D. The damping ratios of the second cycles for the precompressed rubber springs were smaller than 3%, and that was a relatively small damping ratio for damping or self-centering devices.

In general, elastomer or rubber material is prone to be soft due to high temperature. The elastic modulus of the rubber springs may be degraded in high temperature. If that

is the case, the rubber spring behavior could be instable and do not provide sufficient resistance for design. Therefore, a further study to investigate the influence of temperature on the behavior is needed. Further, the rubber springs may be exposed to a broad range of vibration amplitudes. Additional work related to the investigation of fatigue behavior of the rubber springs should be done, in order to provide allowable deformation-based fatigue design criteria.

Acknowledgements

References

Alipour, A., kadkhodaei, M. and Safaei, M. (2017), "Design, analysis, and manufacture of a tension-compression self-centering damper based on energy dissipation of pre-stretched superelastic shape memory alloy wires", *J. Intel. Mat. Syst. Str.*, **28**(15), 2129-2139.

Attanasi, G. and Auricchio, F. (2011), "Innovative superelastic isolation device", *J. Earthq. Eng.*, **15**(1), 72-89.

Bhuiyan, A.R. and Alam, M.S. (2013), "Seismic performance assessment of highway bridges equipped with superelastic shape memory alloy-based laminated rubber isolation bearing", *Eng. Struct.*, **49**, 396-407.

Choi, E., Lee, H.P., Kim, S.I. and Kim, L.H. (2006), "Variation of natural frequency and dynamic behavior of railway open-steel-plate-girder bridge with installing disk bearings", *J. Korean Soc. Steel Struct.*, **18**(4), 437-446.

Choi, E., Youn, H., Park, K. and Jeon, J.S. (2017), "Vibration tests of precompressed rubber springs and a flag-shaped smart damper", *Eng. Struct.*, **132**, 372-382.

Desfuli, H.F. and Alam, M.S. (2013), "Multi-criteria optimization and seismic performance assessment of carbon FRP-based elastomeric isolator", *Eng. Struct.*, **49**, 525-540.

Dhar, S., Das, S. and Saha, P. (2015), "State of art review of shape memory alloy used in civil structures as seismic control device", *Int. J. Res. Technol.*, **4**(13), 195-203.

Dolce, M., Cardone, D. and Marnetto, R. (2000), "Implementation and testing of passive control devices based on shape memory alloys", *Earthq. Eng. Struct. D.*, **29**, 945-968.

Dolce, M., Cardone, D., Ponzo, F.C. and Valente, C. (2005), "Shaking table tests on reinforced concrete frames without and with passive control systems", *Earthq. Eng. Struct. D.*, **34**, 1687-1717.

Fang, C., Yam, M., Lam, A. and Zhang, Y. (2015), "Feasibility study of shape memory alloy ring spring systems for self-centering seismic resisting devices", *Smart Mater. Struct.*, **24**, 075024.

Gao, N., Jeon, J.S., Hodgson, D. and DesRoches, R. (2016), "An innovative seismic bracing system based on a superelastic shape memory alloy ring", *Smart Mater. Struct.*, **25**, 055030.

Hwang, J.S., Wu, J.D., Pan, T.C. and Yang, A. (2002), "A mathematical hysteretic model for elatomeric isolation bearings", *Earthq. Eng. Struct. D.*, **31**, 771-789.

Jeong, K., Choi, E., Back, Y.S. and Kang, J.W. (2016), "Smart damper using sliding friction of Aramid brake lining and self-centering of rubber springs", *Int. J. Steel Struct.*, **16**(4), 1239-

1250.

Kan, Q., Yu, C., Kang, G., Li, J. and Yan, W. (2016), "Experimental observation on rate-dependent cyclic deformation of super-elastic NiTi shape memory alloy", *Mech. Mater.*, **97**, 48-58.

Kikuchi, M. and Aiken, I.D. (1997), "An analytical hysteresis model for elastomeric seismic isolation bearings", *Earthq. Eng. Struct. D.*, **26**, 215-231.

Kim, C.W., Kawatani, M. and Hwang, W.S. (2004), "Reduction of traffic-induced vibration of two-girder steel bridge seated on elastomeric bearings", *Eng. Struct.*, **26**, 2185-2195.

Koblar, D., Skofic, J. and Boltezar, M. (2014), "Evaluation of the Young's modulus of rubber-like materials bonded to rigid surfaces with respect to poisson's ratio", *J. Mech. Eng.*, **60**(7-8); 508-511.

Oh, S.W., Choi, E. and Jung, H.Y. (2005), "The estimated stiffness of rubber pads for railway bridges", *J. Korean Soc. Steel Struct.*, **17**(3), 370-316.

Oh, S.W., Choi, E., Young, J.H. and Kim, H.S. (2006), "Static and dynamic behavior of disk bearings under railway vehicle loading", *J. Korean Soc. Steel Struct.*, **18**(4), 469-480.

Ozbulut, O.E. and Hurlebasu, S. (2011), "Recentering variable friction device for vibration control of structure subjected to near-field earthquakes", *Mech. Syst. Signal Pr.*, **25**, 2849-2862.

Pauletta, M., Cortesia, A. and Russo, G. (2015), "Roll-out instability of small size fiber-reinforced elastomeric isolators in unbonded applications", *Eng. Struct.*, **102**, 358-368.

Qi, H.J. and Boyce, M.C. (2005), "Stress-strain behavior of thermoplastic polyurethane", *Mech. Mater.* , **37**, 817-839.

Qiu, C. and Zhu, S. (2017), "Shake table test and numerical study of self-centering steel frame with SMA braces", *Earthq. Eng. Struct. D.*, **46**, 117-137.

Reedlunn, B., Daly, S. and Shaw, J. (2013), "Superelastic shape memory alloy cables: Part I – Isothermal tension experiments", *Int. J. Solids Struct.*, **50**, 3009-3026.

Soul, H. and Yanwy, A. (2015), "Self-centering and damping capabilities of a tension-compression device equipped with superelastic NiTi wires", *Smart Mater. Struct.*, **24**, 075005.

Strauss, A., Apostolidi, E., Zimmermann, T., Gerhaher, U. and Dritsos, S. (2014), "Experimental investigation of fiber and steel reinforced elastomeric bearings: Shear modulus and damping coefficient", *Eng. Struct.*, **75**, 402-413.

CC